Journal of the Taiwan Institute of Chemical Engineers 150 (2023) 105063

Contents lists available at ScienceDirect

Journal of the Taiwan Institute of Chemical Engineers

journal homepage: www.journals.elsevier.com/journal-of-the-taiwan-institute-of-chemical-engineers

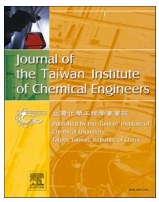

Microfluidic preparation of thin film composite hollow fiber membrane modules for water nanofiltration: Up-scaling, reproducibility and MOF based layers

Javier Esteras-Saz [a,b], Lorena Paseta [a,b], Carlos Echaide-Górriz [a,b], Magdalena Malankowska [a,b], José M. Luque-Alled [a,b], Beatriz Zornoza [a,b], Carlos Téllez [a,b], Joaquín Coronas [a,b,*]

[a] Instituto de Nanociencia y Materiales de Aragón (INMA), CSIC-Universidad de Zaragoza, Zaragoza 50018, Spain
[b] Chemical and Environmental Engineering Department, Universidad de Zaragoza, Zaragoza 50018, Spain

ARTICLE INFO

Keywords:
Hollow fiber membrane module
Microfluidics
Interfacial polymerization
Thin film composite membrane
MOF
Nanofiltration

ABSTRACT

Background: The commercialization of thin film composite (TFC) hollow fiber (HF) membranes remains challenging owing to issues associated with membrane manufacturing.
Methods: TFC membranes were synthesized by microfluidic interfacial polymerization of polyamide (PA) on polysulfone hollow fiber (HF) membrane modules. A total of 33 HF membrane modules were prepared with different number of HFs (from 1 to 25) and different lengths (from 10 to 50 cm). They were evaluated in a nanofiltration operation in terms of water permeance and rose Bengal (RB) and $MgSO_4$ rejections.
Significant findings: Among the 33 modules, 73% showed RB rejections higher than 95%, while 36% of the modules reached rejections above 99%. During the membrane synthesis, different parameters, such as PA monomer concentration, residence time and reaction time, were studied. As a result, the amount of monomer was reduced by ca. 80%. The versatility of microfluidics allowed incorporating hydrophilic metal-organic framework (MOF) ZIF-93 to produce HF modules with PA/MOF bilayered membranes (a continuous layer of MOF between the support and the PA film) which led to an important enhancement of the water permeance from 1.3 (bare PA membrane) to 5.3 $L{\cdot}m^{-2}{\cdot}h^{-1}{\cdot}bar^{-1}$ (PA/ZIF-93 HF membrane), maintaining RB rejection above 95%.

1. Introduction

Water pollution has become a major issue in modern societies due to overpopulation, intense industrialization and lack of appropriate technology for water remediation. Water is typically involved in several industrial processes resulting in the discharge of large amounts of contaminated wastewater into rivers, lakes and seas. Among typical water pollutants, low molecular weight organic compounds are particularly a matter of concern as they are challenging to remove and most of them have been proven harmful to the environment or classified as carcinogenic or mutagenic to humans [1]. The textile industry has been targeted due to its high activity (around $7{\cdot}10^5$ tons of dyes are produced worldwide every year [2]) and its high water consumption (approximately 300 tons of water are employed for manufacturing 1 ton of textile product [3]). Other relevant industries, such as those dealing with rubber, leather tanning packaging, paper and plastic, also produce a large amount of pollutant dyes [4]. Water nanofiltration (NF) stands out as a promising alternative to reduce energy consumption in several industrial processes that require the separation of low molecular weight solutes, including dyes from the textile industry. Moreover, reducing energy input is critical to ensure low carbon emissions and minimize production costs. The energy efficiency of the separation process, and therefore the economics entitled to it, is closely related to the membrane performance. An increment in water permeance while maintaining rejection close to 100% is sought, since this can increase the process productivity at the same energy cost or decrease the energy needed for the process by reducing the pressure required.

Generally, thin film composite (TFC) membranes, consisting of a thin selective polymer film (typically polyamide (PA) for NF and reverse osmosis (RO) applications) deposited on top of a porous support, are employed since these structures give an outstanding performance with high permeances and rejections. Hollow fiber (HF) TFC membranes offer

* Corresponding author at: Instituto de Nanociencia y Materiales de Aragón (INMA), CSIC-Universidad de Zaragoza, Zaragoza 50018, Spain.
E-mail address: coronas@unizar.es (J. Coronas).

https://doi.org/10.1016/j.jtice.2023.105063
Received 17 February 2023; Received in revised form 18 July 2023; Accepted 18 July 2023
Available online 25 July 2023

several advantages over the conventional flat sheet TFC membranes assembled in spiral wound modules. Due to a more efficient occupation of the module space, HFs allow for higher packing density (of up to ca. 10,000 $m^{2}{\cdot}m^{-3}$) and then larger membrane area to volume ratios are achieved. HF membrane modules do not require flow channels, known as "spacers", which saves materials and reduces capital and maintenance costs [5]. It is well accepted that a major cause of fouling in spiral wound modules is due to the presence of such spacers. Albeit fouling also occurs in HF modules, it is generally less severe than in the spiral wound configuration [6]. Besides, backwashing of the membrane to alleviate fouling is easier in a HF configuration (in both inner- and outer-selective TFC membranes) since both the permeate and feed side of the membrane are accessible, whereas spiral wound modules suffer from limited access to the membrane surface and cleaning is difficult [7]. Despite these advantages, the commercialization of TFC HF membranes remains challenging owing to issues associated with membrane manufacturing [8,9]. PA TFC membranes are prepared by a two-step interfacial polymerization (IP) process involving the reaction between an amine, typically m-phenylenediamine (MPD) or piperazine (PIP), dissolved in water and trimesoyl chloride (TMC) monomer dissolved in hexane. In consequence, first steps entail the coating of the support with MPD molecules and the second step consists of the reaction between TMC and the impregnated MPD [10]. Non-uniform distribution of MPD monomers during the coating step or uncompleted reaction in the polymerization step may result in the formation of undesirable defects compromising the membrane performance, as well as its reproducibility and up-scale [5,11]. This can be particularly critical when the PA is synthesized inside of a HF, where to achieve a proper reaction microfluidic contact is needed, as discussed in the next paragraph.

TFC selective films can be prepared in either the outer or inner side of the HF membrane support. Therefore, two main strategies for the synthesis of the PA film have been reported: i) immersing the HFs in a solution containing the monomers [12], and ii) forcing the monomer solutions to travel through the lumen of the HF by a microfluidic approach using syringe pumps [13]. In similar synthesis conditions to those applied for flat supports (i.e. with an easy access of the interfacial polymerization reactant to the support surface), outer-TFC selective layer membranes allow for the preparation of HFs with thinner inner and outer diameters increasing the packing efficiency and the overall surface area per unit volume [8]. On top of that, outer-selective TFC HF membranes suffer from a lower pressure drop and then are less prone to fiber blockage during the manufacturing process than inner-selective TFC HFs [8]. On the contrary, inner-selective TFC layers are easier to manufacture, particularly for large scale modules, save reactants and have better hydraulic flow conditions, lower concentration polarization and suffer from less fouling as compared to outer TFC HFs [8,14]. Recently, it has been shown that the inner TFC HF membrane can be advantageous in terms of NF performance when compared to the TFC prepared on the more porous and rougher outer surface of the same polysulfone (PSF) HF supports [15].

Several works have reported on the synthesis of inner-selective TFC HF membranes of numerous fibers (ranging from 4 to 10 fibers) with ID/OD dimensions of 0.25–1.05 mm/0.38–1.38 mm and of relatively small length (varying from 3 to 18 cm) for pressure-driven water purification [14–17]. Membrane modules with a much larger number of HFs can be prepared as well, for instance, ca. 15 cm-long modules of 200 inner-selective TFC HF membranes have been reported [11,18].

However, the production of large-scale (higher number of long fibers) HF membranes is one of the main challenges in this area. Thus, a robust, simple and reproducible manufacturing process is still lacking. The use of microfluidic technology as an alternative to traditional discontinuous batch reactions leads to higher intensification and productivity since the microfluidic procedure allows for higher control of the interfacial polymerization reaction in the inner surface of the HF protecting the skin layer [15,17,19-22]. While it is true that microfluidics itself has not yet been able to scale-up hollow fiber membranes in terms of length, typically reporting values less than 20 cm, it allows for accurate control of the manufacturing process, making easier to increase knowledge about it.

Besides, this technology can be implemented for the continuous production of metal-organic framework (MOF) layers with accurate control in the synthesis parameters, and thus providing an important step forward towards process intensification closer to scale-up [23,24]. MOF are porous crystalline materials recently implemented as components to enhance the separation performance of membranes in both gas [25] and liquid [26] phases. In fact, the use of nanomaterials integrating a thin film nanocomposite (TFN) membrane or a bilayered membrane (i.e. a layer of a certain nanomaterial between the support and the PA layer) is highly attractive to improve the performance of the resulting membranes. For instance, several nanomaterials, such as MOFs [19], graphene oxide [27], carbon quantum dots [17], cup-like macrocyclic molecules [28] and TiO_2 nanoparticles [29], have been incorporated to PA HF membranes to boost their separation performance. Table 1 sums up all water NF multi-fiber HF membrane modules discussed above comparing their main features. As shown in this table, the preparation of modules with large fibers is barely reported, in particular for inner-selective membranes where only one module [30] contains fibers longer than 18 cm. Preparation methods and achieved membrane areas are summarized in Table S1.

This research aims at fabricating and studying the performance of PA thin film composite membrane modules of up to 25 HFs and a ca. 50 cm length prepared on the inner surface of PSF HF supports of ID/OD dimensions of 0.85/1.2 mm to nanofiltrate an aqueous solution containing a low-molecular weight dye, i.e. rose Bengal (RB, 974 Da) and magnesium sulfate salt ($MgSO_4$, 120 Da). The main goal of this work is to develop a simple and robust fabrication method based on microfluidics capable of: (i) overcoming the difficulties of scaling up longer HF modules without compromising an increase in their number, and (ii) being reproducible in terms of NF performance which is assessed by modifying several synthesis parameters, following novel steps that allow for an adequate polymerization process and selective PA layer formation. The optimization of the membrane fabrication method is of great relevance for the industrial implementation of thin film HF membranes. Using microfluidic technology for fabricating TFC membranes offers two complementary benefits: (*a*) a drastic reduction of the amount of reagents and solvent used, and (*b*) a precise control of the skin layer formed. Finally, the effect of the addition of MOF particles, either forming a TFN membrane or creating a PA/MOF bilayered membrane, was evaluated as well. The production of MOFs on a large scale presents a significant challenge. However, the MOFs utilized in this study have been carefully selected concerning their scalability and economic viability, as well as their membrane performance. For instance, ZIF-8 is one of the most studied MOFs, it has been successfully synthesized in large quantities [34], and it is also available as a commercial material (Basolite® Z1200). Moreover, the scalability of ZIF-94, which is isochemical to ZIF-93 but has a different topology, has been also investigated reporting its feasibility for large-scale production [35]. In addition, the amount of MOF needed in a TFN membrane is estimated in the range of a few milligrams per membrane square meter, which would facilitate their future implementation. MIL-101(Cr) and ZIF-8 are renowned MOFs that have been extensively investigated for preparation of TFN membranes with positive results [36]. In addition, other significant aspects, including their scalability and long-term stability under various conditions (e.g. water environments or high temperature operations) have also been studied in previous works [37,38]. In turn, ZIF-93, despite being less popular than the aforementioned MOFs, offers several advantages, including hydrophilicity, good long-term stability, and synthesis under mild conditions, such as room temperature, short reaction times, and cost-effective reagents [39].

Table 1
HF membrane modules designed for water NF applications detailing the selective side, length and number of fibers, inner and outer diameters, chemicals used to prepare the PA selective layer and membrane permeance and rejection. "n/a" means not available.

Ref.	Selective side	Length (cm)	Number of fibers	ID/OD (mm)	Chemicals for the selective layer	Water permeance (LMH·bar^{-1})	Rejection (%)
[2]	Inner	n/a	8	n/a	PIP, TMC	8.5	99.9% Reactive brilliant blue
[5]	Inner	2.5	200	n/a	PIP, TMC	8.93	98.3% $MgSO_4$
[16]	Inner	3	10	0.75 / 1.2	PIP, TMC	6.5	98% $MgSO_4$
[28]	Inner	10	5	1.6 / 1.14	MPD, SDS, TMC and calix[*n*]arene	1.99	97.6% NaCl
[17]	Inner	14	3	n/a	MPD, SDS, TMC and amino functionalized CQDs	8.7	98.9% NaCl
[11]	Inner	15	200	0.58 / 1.13	MPD, SDS, TMC	4.5	98% NaCl
[18]	Inner	15.5	200	0.575 / 1.025	MPD, SDS and TMC	2.78	90% $MgSO_4$
[14]	Inner	18	4	1.05 / 1.38	PEI, SDS, TMC	16.5	96.5% $MgCl_2$
[30]	Inner	100	20	0.8 / 1.3	PIP and TMC	6	99.5% $MgSO_4$
[31]	Outer	15	4	n/a	MPD, Lysine and TMC	18	100% Eriochrome black T
[32]	Outer	16	3	n/a	PIP and TMC	5.1	69% $MgSO_4$
[6]	Outer	16	4	n/a	PIP, TMC	13.8	98.2% Na_2SO_4
[33]	Outer	30	n/a	0.6 / 1.1	MPD, TMC	5.8	95% Reactive black 5
[12]	Outer	40	4	0.8 / 1.06	PIP, TEA and TMC	4.5	92.3% Na_2SO_4

SDS: sodium dodecyl sulfate; CQD: carbon quantum dots; TEA: trimethylamine.

2. Experimental

2.1. Polysulfone hollow fiber supports

The polysulfone (PSF) HF supports used in this work were kindly provided by the membrane manufacturer Polymem (several batches we used along a period of ca. 2 years). They have inner (ID) and outer (OD) diameters of ca. 850 and 1200 μm, respectively, the pore size being around 15–20 nm and 100 nm, referred to the inner and outer surfaces, respectively.

2.2. Preparation of TFC membranes

PSF HFs were configured in membrane modules by placing a bundle of them inside a nylon tube and sealing both ends with an epoxy resin (Araldite). Two module lengths (*L*) were considered: ca. 10 cm, referred as short modules, and ca. 50 cm, referred as long modules. Different fibers were coupled in both short and long modules with a number of fibers (*N*) ranging from 1 to 25.

Prior to the preparation of the polyamide film, each membrane module was blown out with compressed air for 1 min (to achieve the total removing of the polyetilenglycol (PEG) used to adequately preserve the PSF supports during their storage) and then mounted vertically. The synthesis of the polyamide (PA) thin film was carried out at room temperature on the inner surface of the PSF HF modules by interfacial polymerization (IP). All solutions (MPD in water and TMC in n-hexane, see below) or solvent (pure cyclohexane, CHX) phases were fed to the lumen of the fibers from bottom to top of the module by using different syringe pumps for each solution under microfluidic conditions (Fig. 1).

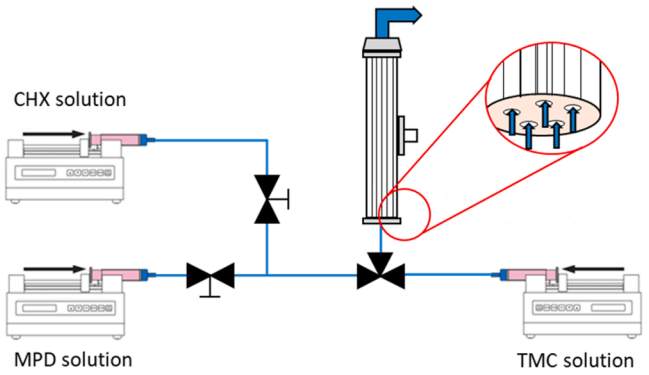

Fig. 1. Scheme of the microfluidic plant.

To synthesize the PA layer, first, a 2%w·v^{-1} (g·mL^{-1}) aqueous solution of MPD (99%, Sigma Aldrich) was fed inside the fibers for 10 min. Then, the module was dried with compressed air for 2 min. Next, an innovative step consisted of pumping a certain volume of pure cyclohexane (Scharlab, extra pure) for 3 min to effectively drain out every trace of the water molecules, avoiding the TMC hydrolysis, and to remove the excess of MPD from the inner side of the fibers. Moreover, a typical curing step under certain temperature was avoided, thereby reducing the energy necessary as compared to previous reports [2,11,16]. A solution of TMC (98%, Sigma Aldrich) in n-hexane (0.01%w·v^{-1}) was then supplied for a certain time using the same fed flow as that used for the MPD solution. Since the reaction between MPD and TMC is considered to be almost instantaneous (i.e. only a few seconds are needed to form the aromatic polyamide), the overall time that the TMC solution is flowing through the fiber is assumed to be the reaction time and this value was varied from 1 to 9 min. Finally, the synthesized PA HFs were cleaned using 20 mL of pure water at 10 mL·min^{-1}. The different synthesis conditions applied are detailed in Table 2. Feed flow was adjusted for modules containing different number of fibers or lengths with the aim of maintaining the residence time unaltered, except in case of condition 4 to evaluate the influence of the residence time. This corresponds to the time that a molecule of MPD, or TMC, resides in the membrane module (i.e. how long the solution takes to travel through the HF) and was calculated as the supplied volume divided by the feed flow. Reaction time corresponds to the time that TMC is in contact with the MPD-impregnated PSF support. Finally, the largest fiber number and length were established according to the limitations of the synthesis rig (mainly available pumps).

2.3. Preparation of TFN and HF PA/MOF bilayered membranes

Two strategies were followed to prepare MOF-containing HF membranes: (*i*) preparation of TFN membranes, where the MOFs were typically dispersed along with TMC in the organic solution prior to the IP reaction, and (*ii*) preparation of PA/MOF bilayered membranes, where a MOF layer was synthesized by direct crystallization on the PSF support followed by IP to polymerize the PA layer [40,41], both MOF and PA synthesized in the lumen side of the HF. Note that, as a proof of concept, membranes containing MOFs were prepared only in modules of *N*: 5, *L*: 10 cm. All MOF-containing HF membranes are summarized in Table 3.

TFN membranes were prepared at room temperature using small amounts of MIL- 101(Cr), i.e., 0.025 and 0.05%w·v^{-1}, and ZIF-8, i.e. 0.025%w·v^{-1}. MIL-101(Cr) and ZIF- 8 nanoparticles (NPs) were

Table 2
Synthesis conditions applied for the TFC HF membrane modules prepared, TMC concentration being always 0.01%w.v^{-1}.

Conditions code	Module code	Area (cm^2)	Feed flow (mL·min^{-1})	Residence time (min)	Reaction time (min)	MPD concentration (%w·v^{-1})
0	**N1L10**	**2.7**	0.19	0.29	9	2
0	**N5L10**	**13.4**	0.96	0.29	9	2
0	**N10L10**	**26.7**	1.93	0.29	9	2
0	**N25L10**	**66.8**	4.82	0.29	9	2
0	**N5L50**	**66.8**	4.82	0.29	9	2
1	**N5L50_C1**	**66.8**	4.82	0.29	4.5	2
2	**N5L50_C2**	**66.8**	4.82	0.29	2.25	2
3	**N5L50_C3**	**66.8**	4.82	0.29	1	2
4	**N5L50_C4**	**66.8**	0.96	1.48	9	2
5	**N5L50_C5**	**66.8**	4.82	0.29	9	1
6	**N25L50_C6**	**334**	24.1	0.29	9	2

Table 3
MOF-containing HF membranes prepared. The PA film was always synthetized according to N5L10 conditions.

Membrane code	MOF addition strategy	MOF	MOF Concentration (%w·v^{-1})
0.025 MIL-101	Dispersed in the organic solution prior de IP reaction (TFN)	MIL-101(Cr)	0.025
0.05 MIL-101		MIL-101(Cr)	0.05
0.025 ZIF-8		ZIF-8	0.025
PA/ZIF-8	Bilayered PA/MOF	ZIF-8	–
PA/ZIF-93		ZIF-93	–

synthesized following the procedures reported by Echaide-Górriz et al. (MIL-101(Cr), ca. 50 nm) [19] and García-Palacín et al., (ZIF-8, ca. 30 nm) [42]. MIL-101(Cr) and ZIF-8 were dispersed in n-hexane using a sonication bath (6 min, 600 W of power) and magnetic stirring (20 min). This treatment consisting of sonication plus stirring was repeated twice and was followed by the application of a sonication tip for 3 min in overall with pulses of 5/3 s on/off (35% of amplitude, 750 W of power and 20 Hz of frequency). Afterwards, the required amount of TMC was added to the MOF-n-hexane dispersion and stirred for 30 min prior to being pumped into the HFs.

For the preparation of the HF PA/MOF bilayered membranes from the second approach, a continuous MOF layer was first formed on the lumen side of the PSF HF support. ZIF-8 and ZIF-93 were selected in this case since they can be easily synthesized by microfluidics at room temperature. ZIF-8 was prepared following a similar procedure to the one developed by Cacho-Bailo et al. [24]. MeOH (Scharlab, 99.9%) at a rate of 0.96 mL·min^{-1} was pumped to wet and to clean the lumen of the HFs. Next, two solutions, one of 0.10 mol·L^{-1} of $Zn(NO_3)_2{\cdot}6H_2O$ (Sigma-Aldrich, 98%) in water and another solution of 0.30 mol·L^{-1} of 2-methylimidazole ($C_4H_6N_2$, Sigma-Aldrich, 99%) and 0.30 mol·L^{-1} of sodium formate (NaCOOH, Sigma-Aldrich, >99%) in methanol, coming from separate syringes (at a rate of 0.48 mL·min^{-1} each), were mixed and forced to go through the lumen of the PSF HFs for 15 min. In comparison to the work of Echaide-Górriz et al. [41] dealing with a PA/ZIF-93 single HF ca. 10 cm long, in this study the amount of TMC employed was reduced by at least 4 times with the consequent saving in reagent costs and lowering of waste generation. Once the MOF layer was formed, 0.96 mL·min^{-1} of MeOH was pumped to remove the excess of unreacted reagents prior to commencing with the IP synthesis procedure detailed in Section 2.2. (TFC membrane preparation). Note that for ZIF-93 crystallization, the same procedure was followed as for ZIF-8 maintaining the same molar ratio Zn^{2+}:linker (1:3), but using a different ligand (i.e. 4-methyl-5-imidazolecarboxaldehyde, $C_5H_6N_2O$, Across-Organics, 99%).

2.4. Membrane characterization

The morphology of the HF membranes was observed by scanning electron microscopy (SEM) using FEI-Inspect™ F20 microscope working at a voltage between 10 and 20 kV. Top-view and cross-section images were acquired. To obtain top-view images of the inner side of the HF membranes, an individual fiber was pulled out from the module, immersed in liquid N_2, and cut longitudinally in half with a scalpel outside of the liquid N_2 to expose the inner side of the fiber. Cross-section images were obtained by immersing the HFs in liquid N_2 and then cutting them transversally.

X-ray diffraction (XRD) characterization was used to analyze the crystallinity of the synthetized MOFs involved in the formation of TFN and PA/MOF bilayered membranes. XRD measurements were taken from 4 to 40° (2θ) with a 0.025°·s^{-1} step using a D-Max 2500 Rigaku diffractometer with a CuKα (λ=0.1542 nm) rotating anode operating at 40 kV and 80 mA.

2.5. Nanofiltration measurements

The performance of the HF membrane modules was assessed in a NF set-up operating in a continuous flow configuration, whose schematic representation is shown in Fig. S1. The feed solution mainly consists of RB (Sigma Aldrich, 95% dye content, 974 Da) as solute at a concentration of 20 mg·L^{-1} and was supplied using a diaphragm pump that allows for a continuous flow configuration at a 6 bar pressure difference (feed-permeate) and 20 °C (RT). The NF set-up has pressure transducers at the feed, retentate and permeate sides, allowing the calculation of the driving force. A Jasco V-670 UV–vis spectrophotometer was used to estimate the RB concentration after the corresponding calibration in the range of concentrations operated. Measurements were carried out at 549 nm, the wavelength of maximum absorbance. Salt rejection capacity of certain membrane modules was also tested to assess an adequate performance of the fabricated modules. To do this, a $MgSO_4$ (120 Da) solution was fed with a concentration of 2 g·L^{-1} instead of the RB solution mentioned. SevenMulti™ pH/conductivity meter (Mettler Toledo) was used to measure the $MgSO_4$ concentration.

Membrane permeance (L·m^{-2}·h^{-1}·bar^{-1}, LMH·bar^{-1}) and rejection (%) values were acquired every hour throughout the whole experiment that lasted for at least 6 h and were calculated as follows:

$$Permeance = \frac{Q}{\Delta P} = \frac{V}{A.t.\Delta P} \quad (1)$$

$$Rejection = \left(1 - \frac{C_{permeate}}{C_{feed}}\right) * 100 \quad (2)$$

where Q is the permeate flux, ΔP is the pressure gradient (calculated as the difference between the feed and retentate average and permeate pressures), V is the volume of permeate collected in a given time t, A is the inner membrane area and $C_{permeate}$ and C_{feed} are the solute

concentrations in both permeate and feed, respectively. Long-term experiments were done removing the membrane modules from the NF setup overnight. During the overnight period (not considered as NF accumulated time) the module was stored under water. NF results were statistically evaluated with one factor analysis of variance, a special case of analysis of variance (ANOVA) at $\alpha < 0.05$ (i.e. with a significant level of 95%), using the Fisher test, where parameter F was calculated facing the variation between groups (i.e., membrane modules with different number of HFs and length) to the corresponding variation within each group (due to unexplained experimental variation). In this case, a significant deviation between the experimental results is confirmed (alternative hypothesis) if experimental F is higher than Fc (F value necessary to reject the null hypothesis with a significant level of 0.05), i.e. the results from different groups are statistically different) [42]. Only membrane modules with rejections higher than 95% were considered in this study; modules with lower rejections were only included for the calculation of the success rate of membrane preparation. Poorer rejections than 95% were accompanied with suspiciously high permeances, consequence of the presence of defects in the PA layer.

3. Results and discussion

3.1. Membrane module manufacturing

Due to the increase in membrane area of the membrane modules (either a greater number of fibers, *N*, or larger fibers, *L*), feed flows of MPD and TMC solutions were adapted according to the total HF inner surface (Table 2), fixing the residence time employed in the development of the first module (**N1L10**, conditions code: 0, residence time: 0.29 min). The up-scaled method allowed increase both number of fibers (*N*; from 1 to 25) and length (*L*; from 10 to 50 cm) without raising the experimental time. Fig. 2 shows photographs of each type of module manufactured. Besides, an increase in the number of HFs still allowed the maintenance of the microfluidic conditions through every single HF, i.e. higher diffusion contribution over convection transport, and working under laminar flow conditions (at Reynolds numbers in the 5 - 36 range, far below 250) [43]. This successfully permitted the extrapolation of the interfacial polymerization synthesis from a unique HF to 25, without losing the membrane quality in terms of NF separation performance as will be shown below.

After the successful initial scale-up (i.e., membrane area increased from 2.7 to 66.8 cm^2), the influence of the synthesis conditions on the module permeance and RB rejection was investigated for the preparation of modules with the largest lengths (N5L50). The following three synthesis parameters were evaluated: *i*) residence time, *ii*) reaction time, and *iii*) MPD concentration. Apart from optimizing these parameters to achieve higher permeances while maintaining the rejection above 95%, changing any of all three parameters mentioned is important to minimize reagents (including both PA monomers and solvents) waste and reduce the overall time of the process, setting also the basis for a potential automation of the membrane module manufacturing. Finally, the incorporation of MOF, either as TFN or as PA/MOF bilayered membranes, was evaluated using a smaller module (N5L10) to proof the concept and minimize the waste of expensive reactants during the study.

3.2. Membrane characterization

Fig. 3A depicts the SEM cross-sectional image of one of the HFs conforming the membrane module where the internal diameter of the fiber along with its thickness can be found in agreement with the previous information given in the experimental section. Fig. 3B shows the top-view images of the inner surface of a fiber from two membrane modules, which differ in their length and number of fibers (N25L10 and N5L50). Besides evidencing the formation of the polyamide, images 1 and 2 in Fig. 3B show that increasing the number of fibers from 1 to 5 did not affect the creation of the typical ridge-and-valley structure characteristic of PA formation by IP [11,19]. These structures are clearly visible in the higher magnification inset corresponding to Fig. 3A. In addition, images 2, 3 and 4 reveal that not significant differences in the PA layer (both thickness and morphology) were observed at three different locations along the HF (images 2, 3 and 4 corresponding approximately to the inflow, middle and outflow). This suggests a homogeneous wetting and polymerization reaction during the IP process along the fiber, refuted when a lower magnification SEM observation covering a larger membrane section was done (see Fig. S2). These SEM images confirm the presence of the PA on top of the porous structure characteristic of membranes prepared by phase inversion.

3.3. Nanofiltration tests

3.3.1. Up-scaling of TFC membranes: number of HFs and their lengths

One of the main challenges in the scale-up process of HF membranes is to increase the fiber length [30]. As the length of the HFs increases, the probability of defect formation grows as the pressure drop markedly increases with length, particularly for inner-selective TFC membranes [11]. Generally, this pressure drop along the fiber results in a more heterogeneous wetting of the support, eventual pore blockage and less effective gas purging (i.e. after MPD impregnation, water drops may remain and produce undesirable defects) [8,11]. However, as it will be shown below, the procedure presented in this study is quite robust and reproducible with fibers up to 5 cm of length. In terms of upscaling to longer modules, it is predicted that an issue concerning pressure drop would be solved by employing more powerful pumps than the ones used here, able to provide higher flow rates. Fig. 4 depicts the permeances and rejection values achieved for the different types of HF membrane modules prepared in the up-scaling study based on the conditions detailed in Table 2. Moreover, the average value of permeance and rejection of the total membrane modules prepared (with different sizes)

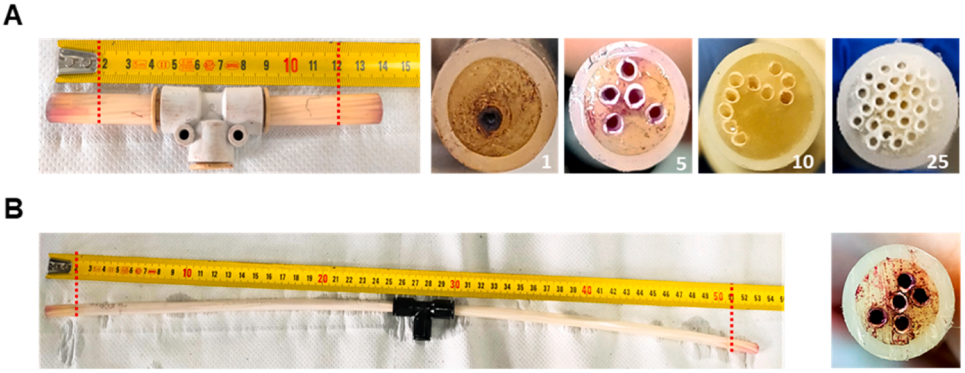

Fig. 2. Photographs of HF membrane modules. (A) $L = 10$ cm; $N = 1$, 5, 10 and 25 fibers; (B) $L = 50$ cm; $N = 5$ fibers.

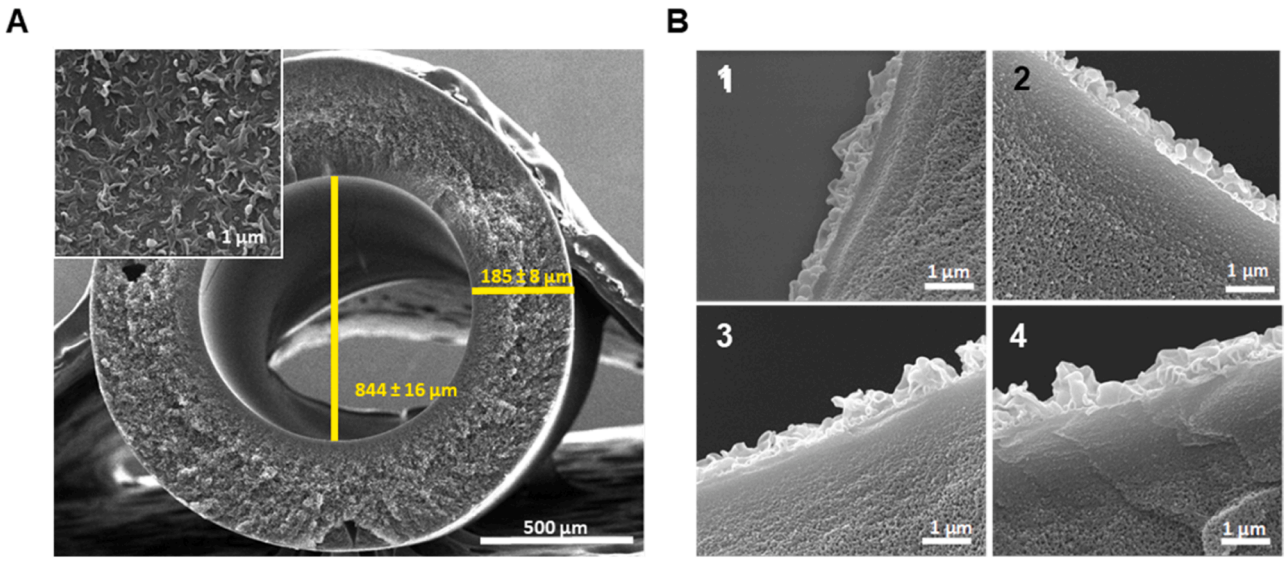

Fig. 3. SEM images. (A) Cross-section of a PSF fiber support. (B) Top-view revealing the inner surface of a HF (after the IP reaction) contained in the membrane modules N1L10 and N5L50; images 2, 3 and 4 correspond to different locations along the HF length: inflow, middle and outflow. See also Figure S2 for lower magnification observation.

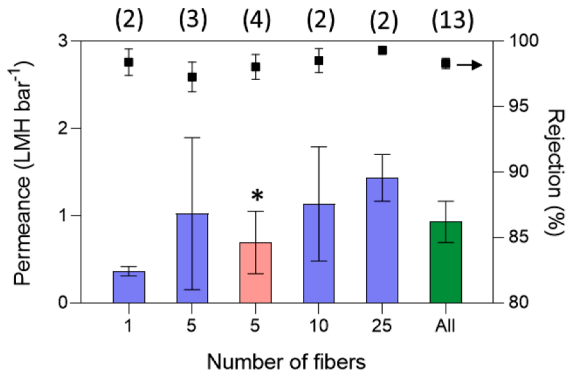

Fig. 4. Water permeance (left) and RB rejection (right) values for all HF membrane modules involved in the up-scaling study as a function of the number of fibers *N* (modules from N1L10 to N25L10, $L = 10$ cm). Red column with asterisk corresponds to $L = 50$ cm, module N5L50, while green one to all the membrane modules. Represented data are the mean values with the corresponding standard deviations. The number of different modules tested is indicated in brackets above their corresponding bar.

is also included in Fig. 4.

As the number of fibers increased in the module (N1L10 to N25L10 in Table 2), the water permeances experienced a rise from ca. 0.4 to 1.4 LMH·bar^{-1}. However, the error bars for all membranes are relatively high and the observed trend must be interpreted cautiously. These results confirm the successful accomplishment of our primary goal, which was to maximize the membrane area in a single HF membrane module using microfluidic technology without compromising the membrane performance (i.e. water permeance and solute rejection). This was certainly achieved as an increment in the number of fibers was not associated with a detriment in the rejection and permanence properties or with a lower success of membrane preparation. Indeed, the overall performance variation observed among the total number of membrane modules [13] was, in general, lower than those observed within each individual membrane module size, thus confirming the high reproducibility of the membrane preparation procedure.

For instance, Table S2 shows that two out of two N25L10 modules (100%) showed RB rejection above 95%, while three out of five N5L10 modules exhibited RB rejection above 95%. Fig. 4 shows that no major differences in water permeance were observed when using different HF lengths and number. The results of the ANOVA test (no significant differences if F < Fc) did not reveal significant differences between the permeance of modules that differed in the number of fibers (F 1.00 < F_c 5.40; $\alpha < 0.05$) or in its length (F 0.49 < Fc 6.60; $\alpha < 0.05$). Salt rejection experiments with $MgSO_4$ solutions (2 g·L^{-1}) were also performed using those membrane modules with higher number (N25L10) and length of fibers (N5L50), previously used for RB separation. As can be inferred from the values of water permeance and salt rejection in Table 4, these results are in line with the smaller size of the $MgSO_4$ [44] and the slight decrease in the rejection values demonstrated the robustness of the synthesis method. Interestingly, module N25L10 showed a slightly better rejection capacity than N5L50, which is consistent with our previous observation with RB. The higher water flux feeding $MgSO_4$ salt solution is in good agreement with the minor rejection achieved as compared to the dye.

3.3.2. *Influence of synthesis parameters: reaction time, MPD concentration, and residence time*

In this section we analyze three of the synthesis parameters used in the IP formation for the up-scaled TFC membranes taking condition 0 (N5L50, Table 2) as a reference. The rejection mechanism of dyes in PA TFC membranes for NF applications typically relies on both size and electrostatic effects. The dense structure of the highly cross-linked PA layer, specifically when utilizing MPD and TMC as monomers, enables sieving capabilities, with transport predominantly governed by a solution-diffusion mechanism. In addition, electrostatic interactions play a significant role in enhancing the rejection properties of membranes due to the presence of several carboxyl groups in the PA layer that leads to electrically charged surfaces. This separation behavior

Table 4
Water permeance and rejection values obtained for RB and $MgSO_4$ solutes with two different membrane modules.

	Permeance (LMH·bar^{-1})		Rejection (%)	
Module	RB	$MgSO_4$	RB	$MgSO_4$
N5L50[a]	0.48 ± 0.07	0.56 ± 0.06	99.1 ± 1.3	84.2 ± 7.6
N25L10[b]	1.25 ± 0.01	1.37 ± 0.11	99.6 ± 0.6	87.8 ± 4.0

[a] module 31 in Table S3.
[b] module 15 in Table S3.

strongly depends on the synthesis conditions employed and on the formation of a highly cross-linked PA layer. As can be seen in Fig. 5A, diminishing the reaction time from 9 to 2 min does not affect the membrane water permeance. Nonetheless, a further decrease in the reaction time down to 1 min led to the formation of a lower-quality PA layer showing larger permeance and lower rejections (1.8 LMH·bar^{-1} and 95%) as compared to the 2 min of the reaction time values (0.86 LMH·bar^{-1} and 99%). We assessed the permeance values for different reaction times using the ANOVA test, which reveals no significant deviation between experimental data ($F\ 3.92 < F_c\ 6.59$; $\alpha < 0.05$). According to these results, 2 min of reaction time seems to be the optimum value as it allows the reduction of the amount of chemicals used without compromising the rejection properties.

Fig. 5B shows the water permeance and RB rejection values for modules that differ in the concentration used of MPD, from 1 to 2% w·v^{-1}, while the TMC concentration was fixed at 0.01%w·v^{-1}. The effect of MPD concentration was observed not to be relevant within the studied range, which is supported by the statistical analysis ($F\ 0.04 < F_c\ 5.99$; $\alpha < 0.05$).

Fig. 5C shows the influence of the residence time in the membrane permeance and rejection. Increasing residence time runs parallel to the decrease of the volumes of MPD and TMC supplied to the membrane synthesis. When the residence time increases from 0.29 to 1.48 min, the water permeance is slightly reduced while the RB rejection remains unaltered; however, the ANOVA test ($F\ 1.28 < F_c\ 7.70$; $\alpha < 0.05$) indicates that there are not statistical differences between both permeance values. The rejection values remained above 97% for all the presented membranes, indicating the absence of any issue related to the non-uniform coating of MPD monomers on the PSF support or incomplete polymerization reactions; except for reaction times shorter than 1 min, which can result in incomplete reactions leading to loosely cross-linked PA layers and subsequent poor rejection rates.

To sum up, a reduction in the use of MPD, TMC and n-hexane up to 80% can be achieved without compromising the NF performance in terms of water permeance and RB rejection of the HF membrane modules. Table 5 details the amount of reagents saved when varying the reaction time, MPD concentration and residence time. By decreasing the reaction time from 9 to 2 min a 78% reduction in TMC and n-hexane solvent used is achieved. The amount of MPD could it be reduced by half, even though 2%w·v^{-1} is often considered as the optimum concentration in most of the studied in the literature [45]. Working at 1.48 min as the residence time resulted in a 5-fold reduction in MPD and TMC consumption, which equates to an 80% reduction in MPD and TMC used.

Considering all the membranes tested in this work, including both up-scaling and synthesis optimization studies, an overall of 33 HF membrane modules with a RB rejection higher than 85% were obtained. Of these, 25 (i.e. 73%) showed a RB rejection above 95% and 12 (i.e. 36%) over 99%. Table S3 contains all the membranes prepared, specifying the corresponding membrane module code (see Table 2), length, number of fibers and condition used. In addition, this table details the

Table 5
Amounts of reagents saved in each modification of the original procedure.

Modification	Amount of reagent saved
Reaction time (from 9 to 2 min)	78% less TMC and n-hexane
MPD concentration (from 2 to 1%w·v^{-1})	50% less MPD and water
Residence time (from 0.29 to 1.48 min)	80% less MPD, water, TMC and n-hexane

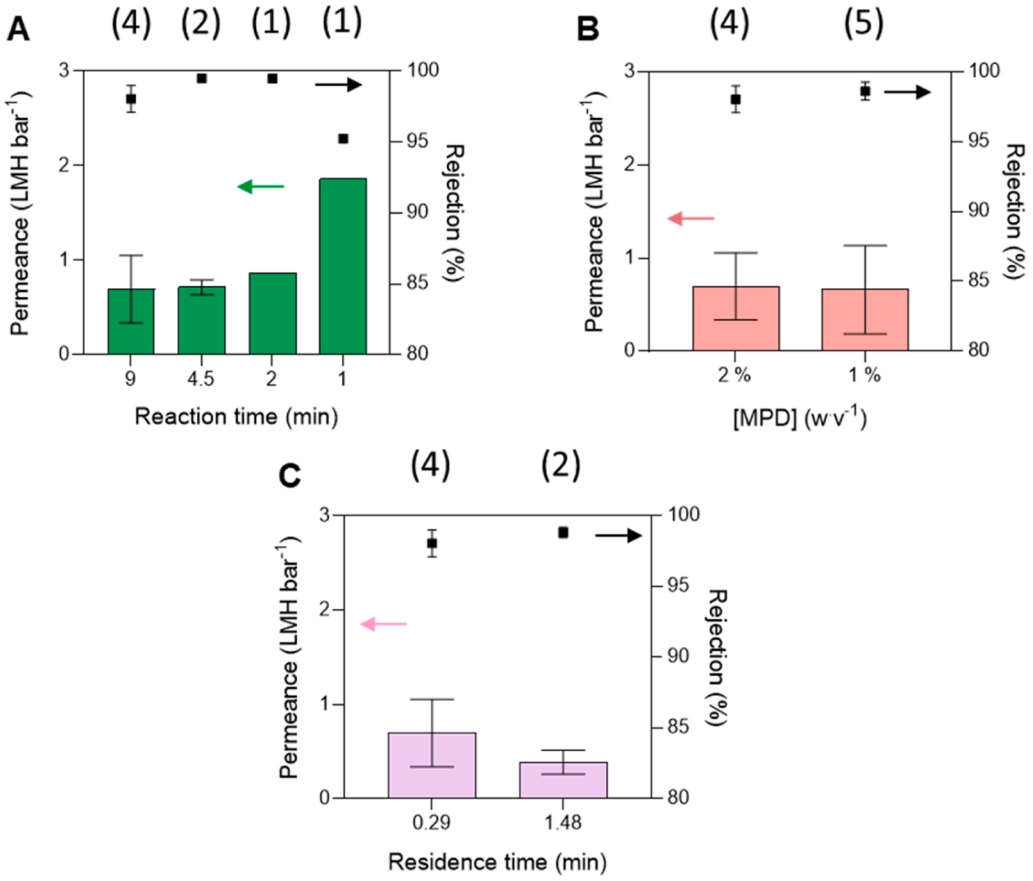

Fig. 5. Water permeance and RB rejection as a function of: (A) reaction time, (B) MPD solution concentration (%w·v^{-1}), and (C) residence time. Represented data are the mean values with their corresponding standard deviations. The number of different membranes tested is indicated in brackets above their corresponding bar. For additional details see Table S4.

number of membranes prepared for this study and specifies how many were successful in terms of NF performance. An interesting fact is that, during the up-scaling study (i.e. considering it as the experiments done with the highest membrane area corresponding to 5 HFs of 50 cm length, N5L50 modules), the overall success rate is around 68% (13 modules out of 19 above 95% RB rejection, see Table S2). Moreover, for the synthesis conditions optimization, the overall success rate is calculated as 78% (11 modules out of 14 above 95% RB rejection, see Table S2). This means that our protocol of PA synthesis using microfluidics is quite robust and slight variations in the amounts of reagents used or times used for each step do not compromise the performance of the membrane modules. Finally, due to the capacity of the syringe pumps, the limit of the up-scaling carried out in this work corresponds to the N25L50 module with 25 HFs of the highest length of 50 cm. Its NF operation is discussed in the next section.

3.3.3. *Stability evaluation by long-term studies on fresh and stored modules*

Selected membrane modules were tested for dye NF as a function of time up to ca. 90 h of accumulated operation (Fig. 6). In particular, the N25L50 module (green down-pointing triangle) with the highest membrane area achieved of 334 cm^2 (see Table 2) was prepared and tested for 40 h without interruption. Water permeance and dye rejection remained pretty stable for the whole period studied. Moreover, two N5L50 modules (blue and orange symbols) were prepared with the same synthesis conditions, measured and stored (under deionized water) for up to one year to also evaluate the possible influence of such circumstances on their NF performance. The open symbols represent the water permeance and rejection of the fresh membranes, the vertical dot line in the graph indicates that the membrane modules were stored for a certain period, and the solid symbols correspond to continuous operation after storage. Regarding the similar initial performance of both N5L50 modules (open symbols), the small discrepancy in water permeance observed in Fig. 6 is within the expected range (0.70 ± 0.36 LMH·bar^{-1}), according to the available standard deviation values. This suggests that this discrepancy might be related with the experimental deviations, that are intrinsic from the manufacturing process of the membrane modules and from the membrane performance measurements, and not with the storage time.

The first N5L50 (purple up-pointing triangle) was prepared and freshly measured (data at 4 h). Then, it was removed from the NF crossflow system, stored in water for 180 days, and mounted again in the rig for testing. A slight decrease in water permeance is observed in Fig. 6 after the storage period from 0.52 LMH·bar^{-1} to 0.41 LHM·bar^{-1} with the RB rejection remaining fairly stable at ca. 98%. Similarly, the other N5L50 module (green down-pointing triangle) was measured right after preparation, stored for 360 days and measured again. After the storage period the variation in water permeance was minimum from 0.79 LMH·bar^{-1} for the fresh module to 0.78 LHM·bar^{-1} for the aged one, the RB rejection maintaining almost constant at ca. 99%. After 68 h of uninterrupted operation, the water permeance stabilized at 0.68 LHM·bar^{-1}, which may be related to a slight fouling of the membrane caused by dye sorption [46,47]. Dye adsorption in the studied HF membranes is far from the reported by other authors where fouling phenomenon led to a flux reduction up to 15% in much shorter periods of time than those studied here [48,49]. This can be explained by the chemistry of the dye, a hydrophilic negatively charged organic molecule, which seems not to closely interact with the negatively charged surface of the PA membrane. To confirm this hypothesis, a hollow fiber membrane module was submitted to backwashing, a standard cleaning procedure, feeding distilled water up to an overpressure of 2 bar during 5 min, showing a back-flux of 4.4 ± 0.4 LMH·bar^{-1}. As shown in Table S5, the membrane module cleaned by backwashing process showed a similar performance in terms of water permeance (0.48 LMH·bar^{-1}) to that shown before backwashing treatment (0.50 LMH·bar^{-1}). This demonstrates a negligible impact of fouling under the experimental conditions used here and also confirms an adequate mechanical resistance of the membrane modules. All these results suggest that the storage of the modules for long periods does not significantly affect their NF performance.

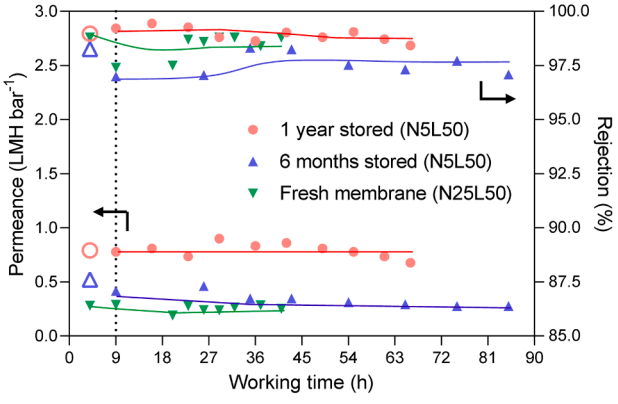

Fig. 6. Long-term NF experiments with RB in water. The vertical line indicates the separation performance before and after storage of the modules. The continuous lines are guides to the eyes.

3.3.4. *Incorporation of MOFs: TFN and PA/MOF bilayered membranes*

MOFs were also incorporated in the TFC HF membranes with the aim of increasing their water permeance while maintaining high dye rejections [19]. As MOFs MIL-101(Cr) and ZIF-8 for the preparation of TFN membranes were obtained as in our previous works, we refer the reader to the corresponding publications for further characterization such as XRD crystallinity, thermogravimetry and textural properties, the relevant particle size values being 50 and 30 nm, respectively [19,42]. In addition, Fig. S3 shows the XRD pattern and SEM images of ZIF-93 that has been synthesized during the formation of the PA/MOF bilayered membranes. That is, during the crystallization of the MOF layer some NPs are deposited on the inner side of the HF support, constituting a more or less continuous layer of intergrown MOF crystals, while some NPs elute from the HFs, then, the latest were collected and analyzed by XRD and SEM. The XRD pattern of the obtained NPs matches the simulated pattern of ZIF-93 (with the RHO type structure [50]) which proves that these NPs correspond to ZIF-93. The SEM image depicts cubic ZIF-93 NPs, ca. 400–800 nm in size. Moreover, Fig. S4 shows SEM images of the inner side of the fiber containing ZIF-93 synthesized on top of the PSF support (prior to synthesizing the PA layer) of similar size to those found in Fig. S3, which confirms that ZIF-93 was successfully deposited at a high surface coverage ratio. Finally, Fig. S5 reveals the typical ridge-and-valley PA morphology, similar to the one presented above for the non-containing MOF membranes (Fig. 3A), but this time on top of the MOF.

Fig. 7 shows the water permeance and RB rejection values of all the MOF-containing membranes prepared in this work. All the TFN membranes (0.025 and 0.05%w·v^{-1} of MIL-101(Cr) and 0.025%w·v^{-1} of ZIF-8) exhibit lower permeance values as compared to that of the original TFC membrane. However, these slight variations between TFC and TFN membranes can be attributed to experimental errors and explained by the standard deviation of the membranes. Similar results were previously noted when using TFNs comprising PA and ZIF-93 [40,51]. In the case of HF membranes prepared in this manuscript, this phenomenon could also be explained due to the presence of very small quantities of MOFs within the PA layer. A frequent issue during the formation of the TFN membrane on the HF membrane modules was the partial blockage of the tubing used to supply the TMC/MOF solution, which was attributed to the agglomeration of MOFs. This suggests that the distribution of the MOF NPs across the five HFs was not properly accomplished (contrarily to the situation with only one HF [19]) and would raise concerns about the homogeneous presence of MOF in all the HFs of the final membrane module. Alternatively, the formation of PA/MOF

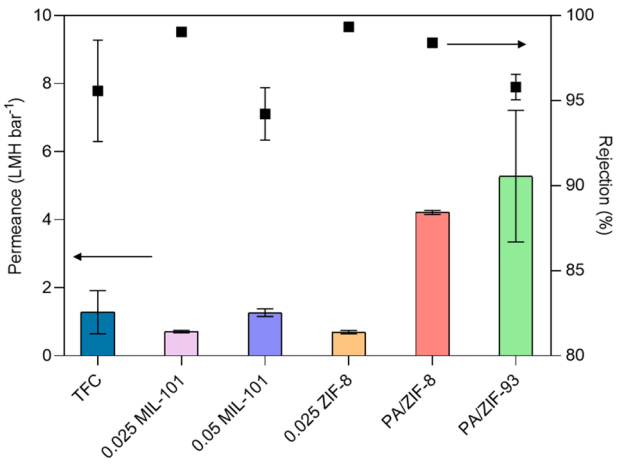

Fig. 7. NF performance of MOF containing N5L10 HF membrane modules: TFC, TFN (0.025 and 0.05%w·v^{-1} of MIL-101(Cr) and 0.05%w·v^{-1} of ZIF-8) and bilayered (PA/ZIF-8 and PA/ZIF-93). Error bars for TFC and PA/ZIF-93 correspond to three different membranes prepared and tested under the same conditions. For the other MOF-containing membranes, error bars correspond to analytical deviations with only one membrane sample.

bilayered membranes was carried out as this allows the crystallization of MOFs on the inner surface of the support which prevents MOF agglomeration and therefore decreases the likelihood of tubing blockage. PA/ZIF-8 and PA/ZIF-93 bilayered membrane modules show permeances of 4.2 and 5.3 LMH·bar^{-1}, respectively, which are much higher than that of the TFC HF membrane module of the same dimensions (1.3 LMH·bar^{-1}). This increase in water permeance due to the existence of a MOF sublayer has been thoroughly investigated in our previous work [40,51]. The presence of the sublayer results in thinner PA layers and increased surface roughness, which leads to a higher membrane surface area. The PA/ZIF-93 module exhibits a slightly higher permeance than the PA/ZIF-8 one, which can be attributed to the hydrophilic nature of ZIF-93 (due to the aldehyde group in the imidazolate ligand [40,51]) as compared to ZIF-8. The effects of the ZIF-93 sub-layer on the NF results have been observed in previous works and have been related to a lower thickness of the PA layer, increased hydrophilicity due to the hydrophilic character of the MOF and increased roughness, without in any case affecting the quality of the PA layer [41,51,52]. Rejection values for both PA/ZIF bilayered membranes (98.4 and 95.8% for ZIF-8 and ZIF-93, respectively) are comparable to that of the TFC HF membrane module (95.6%).

4. Conclusions

Our results demonstrate that TFC and PA/MOF bilayered membrane modules of varying lengths and number of hollow fibers can be successfully prepared using a simple, robust and reproducible approach based on microfluidics. TFC HF membranes can be up-scaled in number of fibers (from 1 to 25) and in module length (from 10 to 50 cm). An evaluation of three parameters of the PA synthesis (i.e., TMC reaction time from 9 to 2 min, MPD concentration from 2 to 1%w·v^{-1} and residence time from 0.29 to 1.48 min) allows a significant reduction, up to 80% in case of increasing the residence time, of the amount of chemicals employed and waste generated during the synthesis without compromising the membrane NF performance. In fact, comparing the amounts spent here with those typically reported in the literature for the formation of inside PA hollow fibers, the achieved reductions were 35 and 127 times for amine and TMC (inferred from the available data from similar works shown in Table S1). It is evident that a lower expenditure of reagents will help in the scaling-up of the HF membrane modules.

Fabrication of PA/ZIF bilayered membranes led to a significant enhancement in water permeation. In particular, PA/ZIF-93 bilayered membrane module, due to the hydrophilic character of the MOF used, exhibited around 400% enhancement in water permeance as compared to TFC HF membrane modules. The ca. 90 h long-term nanofiltration demonstrated that one year stored HF membrane modules did not show significant loss of performance.

Even if some work remains for the future (increasing more the number of HFs/HF length/membrane module area, testing more different solutes, addressing potential membrane refreshing conditions, studying more in detail the performance of the TFN membranes, etc.), this study opens the door for synthesizing MOF containing HF membrane modules with more precise control of selective skin layers and sparing reagents, thus representing a promising step towards the more sustainable process intensification of both the fabrication of the membranes and their effective implementation in NF for the removal of water pollutants.

Declaration of Competing Interest

The authors declare that they have no known competing financial interests or personal relationships that could have appeared to influence the work reported in this paper.

Acknowledgments

This work has been performed in the frame of the INNOMEM project that has received funding from the European Union's Horizon 2020 Research and Innovation Program under Grant Agreement N° 862330. In addition, financial support from the Research Project PID2019-104009RB-I00/AEI/10.13039/501100011033, the Aragón Government (T68-23R), and the ESF are gratefully acknowledged. J. M. Luque-Alled acknowledges the Spanish Ministerio de Universidades and the European Union-NextGenerationEU Fund for funding through the Margarita Salas and Juan de la Cierva programmes. The authors acknowledge the LMA and Servicio General de Apoyo a la Investigación (SAI, Universidad de Zaragoza) for offering access to their instruments and expertise. We also acknowledge Polymem Membrane Manufacturer for the PSF hollow fibers.

Supplementary materials

Supplementary material associated with this article can be found, in the online version, at doi:10.1016/j.jtice.2023.105063.

References

[1] Khattab TA, Abdelrahman MS, Rehan M. Textile dyeing industry: environmental impacts and remediation. Environ Sci Pollut Res 2020;27(4):3803–18.
[2] Wei XZ, Kong X, Sun CT, Chen JY. Characterization and application of a thin-film composite nanofiltration hollow fiber membrane for dye desalination and concentration. Chem Eng J 2013;223:172–82.
[3] El-Dein AM, Libra J, Wiesmann U. Cost analysis for the degradation of highly concentrated textile dye wastewater with chemical oxidation H2O2/UV and biological treatment. J Chem Technol Biotechnol 2006;81(7):1239–45.
[4] Feng XQ, Peng DL, Zhu JY, Wang Y, Zhang YT. Recent advances of loose nanofiltration membranes for dye/salt separation. Sep Purif Technol 2022:285.
[5] Yang TS, Wang KY, Chung TS. Fabrication of thin-film composite hollow fiber membranes in modules for concentrating pharmaceuticals and separating sulphate from high salinity brine in the chlor-alkali process. J Membr Sci 2021:640.
[6] Wang CF, Chen YB, Hu XY, Guo PF. Engineering novel high-flux thin-film composite (TFC) hollow fiber nanofiltration membranes via a facile and scalable coating procedure. Desalination 2022:526.
[7] Sengur-Tasdemir R, Urper-Bayram GM, Turken T, Ates-Genceli E, Tarabara VV, Koyuncu I. Hollow fiber nanofiltration membranes for surface water treatment: performance evaluation at the pilot scale. J Water Process Eng 2021:42.
[8] Choi O, Peck DH, Park CH. High-performance nanofiltration of outer-selective thin-film composite hollow-fiber membranes via continuous interfacial polymerization. J Ind Eng Chem 2021;103:373–80.
[9] Schwinge J, Neal PR, DE Wiley, Fletcher DF, Fane AG. Spiral wound modules and spacers - review and analysis. J Membr Sci 2004;242(1–2):129–53.
[10] Cadotte JE, Petersen RJ, Larson RE, Erickson EE. New thin-film composite seawater reverse-osmosis membrane. Desalination 1980;32(1–3):25–31.

[11] Yang TS, Wan CF, Zhang JY, Gudipati C, Chung TS. Optimization of interfacial polymerization to fabricate thin-film composite hollow fiber membranes in modules for brackish water reverse osmosis. J Membr Sci 2021:626.
[12] Liu JQ, Xu ZL, Li XH, Zhang Y, Zhou Y, Wang ZX, et al. An improved process to prepare high separation performance PA/PVDF hollow fiber composite nanofiltration membranes. Sep Purif Technol 2007;58(1):53–60.
[13] Verissimo S, Peinemann KV, Bordado J. Thin-film composite hollow fiber membranes: an optimized manufacturing method. J Membr Sci 2005;264(1–2):48–55.
[14] Fang WX, Shi L, Wang R. Interfacially polymerized composite nanofiltration hollow fiber membranes for low-pressure water softening. J Membr Sci 2013;430:129–39.
[15] Echaide-Gorriz C, Malankowska M, Tellez C, Coronas J. Nanofiltration thin-film composite membrane on either the internal or the external surface of a polysulfone hollow fiber. AlChE J 2020;66(6):13.
[16] Wang W, Li GD. One-step Fabrication of High Selective Hollow Fiber Nanofiltration Membrane Module. Fibers Polym 2010;11(7):1041–8.
[17] Gai WX, Zhang Y, Zhao QP, Chung TS. Highly permeable thin film composite hollow fiber membranes for brackish water desalination by incorporating amino functionalized carbon quantum dots and hypochlorite treatment. J Membr Sci 2021:620.
[18] Yang TS, Wan CF, Xiong JY, Chung TS. Pre-treatment of wastewater retentate to mitigate fouling on the pressure retarded osmosis (PRO) process. Sep Purif Technol 2019;215:390–7.
[19] Echaide-Gorriz C, Aysa-Martinez Y, Navarro M, Tellez C, Coronas J. Polyamide-MIL-101(Cr) thin films synthesized on either the outer or inner surfaces of a polysulfone hollow fiber for water nanofiltration. ACS Appl Mater Interfaces 2021;13(6):7773–83.
[20] Chen YF, Loh CH, Zhang LZ, Setiawan L, She QH, Fang WX, et al. Module scale-up and performance evaluation of thin film composite hollow fiber membranes for pressure retarded osmosis. J Membr Sci 2018;548:398–407.
[21] Ren J, McCutcheon JR. Making thin film composite hollow fiber forward osmosis membranes at the module scale using commercial ultrafiltration membranes. Ind Eng Chem Res 2017;56(14):4074–82.
[22] Zhang S, Sukitpaneenit P, Chung TS. Design of robust hollow fiber membranes with high power density for osmotic energy production. Chem Eng J 2014;241:457–65.
[23] Echaide-Gorriz C, Clement C, Cacho-Bailo F, Tellez C, Coronas J. New strategies based on microfluidics for the synthesis of metal-organic frameworks and their membranes. J Mater Chem A 2018;6(14):5485–506.
[24] Cacho-Bailo F, Catalan-Aguirre S, Etxeberria-Benavides M, Karvan O, Sebastian V, Tellez C, et al. Metal-organic framework membranes on the inner-side of a polymeric hollow fiber by microfluidic synthesis. J Membr Sci 2015;476:277–85.
[25] Ma YN, Sun YX, Yin J, Sun HS, Wu H, Wang H, et al. A MOF membrane with ultrathin ZIF-8 layer bonded on ZIF-8 in-situ embedded PSf substrate. J Taiwan Inst Chem Eng 2019;104:273–83.
[26] Vinu M, Raja DS, Jiang YC, Liu TY, Xie YY, Lin YF, et al. Effects of structural crystallinity and defects in microporous Al-MOF filled chitosan mixed matrix membranes for pervaporation of water/ethanol mixtures. J Taiwan Inst Chem Eng 2018;83:143–51.
[27] Tian L, Jiang YX, Li SX, Han LH, Su BW. Graphene oxide interlayered thin-film nanocomposite hollow fiber nanofiltration membranes with enhanced aqueous electrolyte separation performance. Sep Purif Technol 2020:248.
[28] Lan NN, Wang KY, Weber M, Maletzko C, Chung TS. Investigation of novel molecularly tunable thin-film nanocomposite nanofiltration hollow fiber membranes for boron removal. J Membr Sci 2021:620.
[29] Urper-Bayram GM, Sayinli B, Sengur-Tasdemir R, Turken T, Pekgenc E, Gunes O, et al. Nanocomposite hollow fiber nanofiltration membranes: fabrication, characterization, and pilot-scale evaluation for surface water treatment. J Appl Polym Sci 2019;136(45).
[30] Li HB, Shi WY, Zhang HX, Zhou R, Qin XH. Preparation of internally pressurized polyamide thin-film composite hollow fiber nanofiltration membrane with high ions selectivity by a facile coating method. Prog Org Coat 2020:139.
[31] Zhang K, Yang K, Chen YB, Hu YX. Ionic and pH responsive thin film composite hollow fiber nanofiltration membrane for molecular separation. Desalination 2020:496.
[32] Turken T, Sengur-Tasdemir R, Sayinli B, Urper-Bayram GM, Ates-Genceli E, Tarabara VV, et al. Reinforced thin-film composite nanofiltration membranes: fabrication, characterization, and performance testing. J Appl Polym Sci 2019;136(39).
[33] Maurya SK, Parashuram K, Singh PS, Ray P, Reddy AVR. Preparation of polysulfone-polyamide thin film composite hollow fiber nanofiltration membranes and their performance in the treatment of aqueous dye solutions. Desalination 2012;304:11–9.
[34] Deacon A, Briquet L, Malankowska M, Massingberd-Mundy F, Rudic S, Hyde TL, et al. Understanding the ZIF-L to ZIF-8 transformation from fundamentals to fully costed kilogram-scale production. Commun Chem 2022;5(1).
[35] Johnson T, Lozinska MM, Orsi AF, Wright PA, Hindocha S, Poulston S. Improvements to the production of ZIF-94; a case study in MOF scale-up. Green Chem 2019;21(20):5665–70.
[36] Sorribas S, Gorgojo P, Tellez C, Coronas J, Livingston AG. High flux thin film nanocomposite membranes based on metal-organic frameworks for organic solvent nanofiltration. J Am Chem Soc 2013;135(40):15201–8.
[37] Burtch NC, Jasuja H, Walton KS. Water stability and adsorption in metal-organic frameworks. Chem Rev 2014;114(20):10575–612.
[38] Park KS, Ni Z, Cote AP, Choi JY, Huang RD, Uribe-Romo FJ, et al. Exceptional chemical and thermal stability of zeolitic imidazolate frameworks. Proc Nat Acad Sci USA 2006;103(27):10186–91.
[39] Ramos-Fernandez EV, Grau-Atienza A, Farrusseng D, Aguado S. A water-based room temperature synthesis of ZIF-93 for CO2 adsorption. J Mater Chem A 2018;6(14):5598–602.
[40] Paseta L, Antoran D, Coronas J, Tellez C. 110th Anniversary: polyamide/metal-organic framework bilayered thin film composite membranes for the removal of pharmaceutical compounds from water. Ind Eng Chem Res 2019;58(10):4222–30.
[41] Echaide-Gorriz C, Zapata JA, Etxeberria-Benavides M, Tellez C, Coronas J. Polyamide/MOF bilayered thin film composite hollow fiber membranes with tuned MOF thickness for water nanofiltration. Sep Purif Technol 2020;236(8).
[42] Garcia-Palacin M, Martinez JI, Paseta L, Deacon A, Johnson T, Malankowska M, et al. Sized-controlled ZIF-8 nanoparticle synthesis from recycled mother liquors: environmental impact assessment. ACS Sustain Chem Eng 2020;8(7):2973–80.
[43] Elvira KS, Solvas XCI, Wootton RCR, deMello AJ. The past, present and potential for microfluidic reactor technology in chemical synthesis. Nat Chem 2013;5(11):905–15.
[44] Berned-Samatan V, Piantek M, Coronas J, Tellez C. Nanofiltration with polyamide thin film composite membrane with ZIF-93/SWCNT intermediate layers on polyimide support. Sep Purif Technol 2023:308.
[45] Seah MQ, Lau WJ, Goh PS, Tseng HH, Wahab RA, Ismail AF. Progress of interfacial polymerization techniques for polyamide thin film (nano)composite membrane fabrication: a comprehensive review. Polymers 2020;12(12).
[46] Hidalgo AM, Leon G, Gomez M, Murcia MD, Gomez E, Macario JA. Removal of different dye solutions: a comparison study using a polyamide NF membrane. Membranes 2020;10(12).
[47] Luque-Alled JM, Abdel-Karim A, Alberto M, Leaper S, Perez-Page M, Huang K, et al. Polyethersulfone membranes: from ultrafiltration to nanofiltration via the incorporation of APTS functionalized-graphene oxide. Sep Purif Technol 2020:230.
[48] Lee J, Zhan M, Kim Y, Hong S. Comparison of different cleaning strategies on fouling mitigation in hollow fiber nanofiltration membranes for river water treatment. J Clean Prod 2022:380.
[49] Kim H, Shim I, Zhan M. Chemical enhanced backwashing for controlling organic fouling in drinking water treatment using a novel hollow-fiber polyacrylonitrile nanofiltration membrane. Appl Sci-Basel 2021;11(15).
[50] Morris W, Leung B, Furukawa H, Yaghi OK, He N, Hayashi H, et al. A combined experimental-computational investigation of carbon dioxide capture in a series of isoreticular zeolitic imidazolate frameworks. J Am Chem Soc 2010;132(32):11006–8.
[51] Luque-Alled JM, Martínez-Izquierdo L, Gorgojo P, Téllez C, Coronas J. Organic solvent-free fabrication of thin film polyamide/zeolitic imidazolate framework membranes for removal of dyes from water. Chem Eng J 2023;470:144233.
[52] Berned-Samatan V, Galan-Gonzalez A, Munoz E, Benito AMM, Maser WKK, Coronas J, et al. Single-walled carbon nanotube buckypaper as support for highly permeable double layer polyamide/zeolitic imidazolate framework in nanofiltration processes. J Membr Sci 2022:652.